Low potential barrier height effects in magnetic tunneling junctions

E. S. Cruz de Gracia,[1] L. S. Dorneles,[2] L. F. Schelp,[2] S. R. Teixeira,[1] and M. N. Baibich[1,*]
[1]*Instituto de Física, UFRGS, Caixa Postal 15051, Porto Alegre, 91501-970 Rio Grande do Sul, Brazil*
[2]*Departamento de Física, UFSM, Santa Maria, 97105-900 Rio Grande do Sul, Brazil*
(Received 29 March 2007; revised manuscript received 14 August 2007; published 26 December 2007)

This paper reports on the study of deposited ($Ni_{81}Fe_{19}/AlO_x/Co$) magnetic tunnel junctions by magnetron sputtering, with the insulating layer obtained by plasma oxidation of Al. Concentration of the tunnel current in small areas of the junctions and low potential barrier heights were identified by fitting, for each individual sample, the room temperature *I-V* curves with either Simmons' [J. Appl. Phys. **34**, 1793 (1963); **35**, 2655 (1964); **34**, 2581 (1963)] or Chow's [J. Appl. Phys. **36**, 559 (1965)] model. A fast decrease of the tunnel magnetoresistance as a function of the bias voltage is observed, with an inversion of its signal above a critical value. The results are discussed in terms of the quantum coherence factor for low height insulating barriers.

DOI: 10.1103/PhysRevB.76.214426 PACS number(s): 75.47.−m, 73.40.Gk

I. INTRODUCTION

Spintronics is a very active field of research on account of its richness in physical phenomena and technological applications. Among the spintronics arrangements, magnetic junctions (MTJs) with spin polarized tunneling are the simplest and are incorporated in nonvolatile magnetic random access memories and sensor heads. Beyond this simple structure, the variation of the tunneling conductivity when external fields are applied, the so-called tunnel magnetoresistance (TMR), involves several physical mechanisms and, in spite of the tremendous number of works in the field, the TMR bias dependence remains not completely understood.

The importance of spin up and/or down densities of states (DOSs) near the electrode/insulator interfaces over the signal, values, and bias dependence of the TMR is well established. Increasing the bias, the conductance increases because it shifts the Fermi level of one electrode with respect to the other, modifying the tunneling states' population. It causes the effective spin polarization (P) and potential barrier height to go down, allowing higher energy states to tunnel easily. A DOS bias dependence thus leads to a TMR bias dependence. A rigorous treatment should consider the complete band structure and not only the DOS at the Fermi level,[1,2] and some difficulties may arise while choosing the relevant spin polarization factor.[3] Even so, the idea has been largely used to reveal the electronic structure of superconductor materials and to explain complex dependencies of the TMR as a function of bias voltage in junctions.[4]

The insulating layer also plays a role in the TMR dependence with bias. According to Zhang and White,[5] a spin-independent two-step tunneling current via defect states in the amorphous barrier could be responsible for the TMR bias dependence. Zhang *et al.*[6] and Cabrera and García[7] showed that this is due to magnon excitations by hot electrons at the electrode/barrier interface, at least for low applied bias ($\leqslant$40 mV). More recently, extensions of Slonczewski's model[8] for finite bias[9–11] have shown that the TMR is a function of the potential barrier height and this dependence can lead to TMR inversion for low enough barrier and large electron effective mass.[12,13] Experimental evidences have been observed in systems with TaO_x barriers.[14]

To approach the effects of barrier height and thickness over the magnetoresistance, an adequate determination of these quantities is crucial. Transmission electron microscopy (TEM) and grazing incidence x-ray reflectivity (GIXR) are powerful tools for thin films thickness determination, but the visualized area for TEM may not be representative of the effective junction area as a whole.[15,16] On the other hand, GIXR determines an average thickness over relatively large areas. In junctions with fluctuations of thickness and/or barrier composition, the tunnel current concentrates in small parts of the junction area,[17–19] designated hot spots, where the barrier thickness and/or height achieve its lowest value. As a consequence, thicknesses obtained from TEM and GIXR are usually higher than those deduced from electronic transport.[20] Buchanan *et al.*,[21] using GIXR, showed that the insulating barrier thickness is, in all cases, much larger than the thickness of the initial Al metallic layer before oxygen incorporation and twice the value determined from the *I-V* curves fittings. As a matter of fact, results for insulating thickness extracted from GIXR, TEM, and *I-V* curves should converge only in small and strictly perfect junctions. In this context, fitting of the *I-V* from model curves is helpful because the current will intrinsically probe the relevant part of the junction.

In the following, we present results on the TMR as a function of applied voltage in $Ni_{81}Fe_{19}/AlO_x/Co$ tunnel junctions. Rather than a slow decrease of the TMR with increasing bias, usually observed in similar systems, we observe a fast drop of the TMR, with an inversion of its signal above a few hundred milivolts. In order to investigate the role played by the insulating layer characteristics over the TMR, we extract the barrier parameters from the *I-V* curves of each individual sample.

II. EXPERIMENT

Samples were deposited from pure (99.99%) bulk targets by magnetron sputtering with typical base pressure of 10^{-7} mbar (or lower) using masks to define 200 μm electrodes in the crossed stripe geometry with a 4×10^{-4} cm^2 junction area. Material stack was deposited on glass substrate and consists of Ta(98)/Py(474)/Al(20)O_x(Y)/Co(420)/

Cu(100), where $Y=30$, 45, and 60 s stand for the oxidation time process (T_{ox}), and all the nominal thickness are in angstroms. The insulating barrier was deposited by glow discharge assisted oxidation of a thin Al (20 Å) film in a 100 mbar O_2 atmosphere.

I-V curves were measured using the four point probe method in a dc low noise system. This system has input impedance greater than 10 GΩ. A standard resistor in series with the sample is used to detect the sample's current flow. A differential instrumentation amplifier then amplifies the measured voltage. MR curves were measured with an ac synchronous detection technique using low frequency signal.

The *M-H* curves for room temperature were measured using an alternating gradient magnetometer. Low temperature measurements were accomplished in a superconducting quantum interference device magnetometer (Quantum Design model MPMS-XL). The temperature (77 K) was settled at zero field cooling at 10 K/min and the system configured for dc measurements.

Fitting procedures

The fitting procedure for the *I-V* curves was done using Simmons'[22–24] and Chow's models.[25] Both models evaluate the tunnel current density using the Wentzel-Kramers-Brillouin (WKB) approximation for tunneling probability, differing on the approach to solve the integrals. While the first approximates the arbitrary potential barrier $\varphi(x,V)$ to a mean barrier height $[\bar{\varphi}(V)]$, the second approximates any arbitrary potential barrier by an equivalent rectangular barrier whose height is determined by the root mean square value of the arbitrary potential barrier. This leads to a dependence of bias polarity for asymmetrical tunnel barriers. In order to compare the tunnel current density with the experimental data, an explicit potential barrier shape must be assumed. Also, while fitting the experimental curves with the models, the junction area was left as an additional free parameter to contemplate the presence of hot spots.[17–20]

For similar electrodes and nonzero temperatures, both models assume a rectangular potential barrier, so the tunnel current densities are given in practical units for Simmons' and Chow's models by

$$J(V,T)=\left(\frac{6.2\times10^{10}}{t^2}\right)\left\{\left(\varphi_0-\frac{V}{2}\right)\times\exp\left[-1.025t\left(\varphi_0-\frac{V}{2}\right)^{1/2}\right]-\left(\varphi_0+\frac{V}{2}\right)\exp\left[-1.025t\left(\varphi_0+\frac{V}{2}\right)^{1/2}\right]\right\}\times\left(1+\left[\frac{3\times10^{-9}t^2T^2}{\left(\varphi_0-\frac{V}{2}\right)}\right]\right) \quad (1)$$

and

$$J(V,T)=\left(\frac{9.2484\times10^{10}}{t^2}\right)\{\varphi_r\exp[-1.025t(\varphi_r)^{1/2}]-(\varphi_r+V)\exp[-1.025t(\varphi_r+V)^{1/2}]\}\times\left(1+\left[\frac{3\times10^{-9}t^2T^2}{\varphi_r}\right]\right), \quad (2)$$

respectively. In the expressions, T stands for temperature and the free parameters are the rectangular potential barrier φ_0 (V), the insulating barrier thickness t (Å), and the junction area A (cm^2) which is related to the measured tunnel current (I) through $J(V,T)=I/A$.

Also, φ_r is the equivalent rectangular barrier height given by

$$\varphi_r=\frac{4}{9}([\varphi_0{}^{3/2}-(\varphi_0-V)^{3/2}]/V)^2. \quad (3)$$

For dissimilar electrodes and nonzero temperatures, both models assume a trapezoidal potential barrier. In this work, we assume the tunnel current density in the reverse direction, that is, electrode 2 (Py) is positively biased with respect to electrode 1 (Co). In practical units for Simmons' and Chow's models, the tunnel currents are given by

$$J_{1\to2}(V,T)=\{(\varphi_1+\varphi_2-V)\exp[-0.7244t(\varphi_1+\varphi_2-V)^{1/2}]-(\varphi_1+\varphi_2+V)\exp[-0.7244t(\varphi_1+\varphi_2+V)^{1/2}]\}\times\left(\frac{3.6537\times10^{10}}{t^2}\right)\left(1+\left[\frac{6\times10^{-9}t^2T^2}{(\varphi_1+\varphi_2-V)}\right]\right) \quad (4)$$

and

$$J_{1\to2}(V,T)=\left(\frac{9.2484\times10^{7}}{t^2}\right)\{\varphi_{r_{12}}\exp[-1.025t(\varphi_{r_{12}})^{1/2}]-(\varphi_{r_{12}}+V)\exp[-1.025t(\varphi_{r_{12}}+V)^{1/2}]\}\times\left(1+\left[\frac{3\times10^{-9}t^2T^2}{\varphi_{r_{12}}}\right]\right), \quad (5)$$

respectively. The parameter $\varphi_{r_{12}}$ is the effective barrier height and is given by

$$\varphi_{r_{12}}=\frac{4}{9}([\varphi_1^{3/2}-(\varphi_2-V)^{3/2}]/[\varphi_1-\varphi_2+V])^2, \quad (6)$$

and φ_1 and φ_2 (free parameters) are the potential barrier heights at the interfaces between the insulating barrier and electrodes 1 and 2, respectively.

It should be noted that all equations are in the intermediate voltage range, that is, $0\leqslant V\leqslant\varphi_0$ for similar electrodes and $0\leqslant V\leqslant\varphi_2$ for dissimilar ones. Also, the potential barrier height has a bias dependence, and when $\varphi_1=\varphi_2$, all equations reduce to similar electrode equations.

III. RESULTS AND DISCUSSION

Figure 1 shows *I-V* curves for a Py/Al(20 Å)O_x(30 s)/Co sample with a linear shape for $V\to0$ and a non-Ohmic behavior above 150 mV. The moderate increases of the low

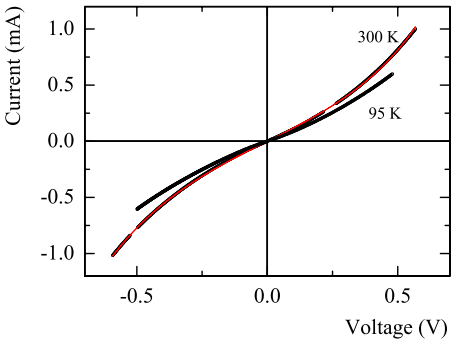

FIG. 1. (Color online) Experimental room temperature *I-V* curve fitted using Chow's model for asymmetrical tunnel barrier showing experimental curve (points) and simulated one (line). The ferromagnetic electrodes are in the parallel state of magnetization. Some experimental points have been left out intentionally to show the quality of the fit. *I-V* curve for 95 K shows a resistance increase with a decrease in temperature.

voltage electrical resistance when the temperature decreases, together with the *I-V* curve shape indicate quantum tunneling as the charge transport mechanism.[26] For $V \to 0$, the first exponential factor in the right hand side of Eq. (5), corresponding to the first quadrant of Fig. 1, has a small contribution, leaving only the linear contribution for the *I-V* characteristic.

For $V \leqslant \varphi_2$, the exponential factor has a larger contribution than the linear one, approximately 1 order of magnitude higher than the normalized value for $V \to 0$, leading to a nonlinear behavior, as can also be seen in Fig. 1.

Physically this means that the bias shifts the Fermi level of one electrode with respect to the other, and the effective barrier height decreases, so more electrons can tunnel because there are more empty states available on the second electrode, increasing the transmission coefficient. As a consequence, the barrier resistance decreases. Figure 2 shows a schematic energy diagram illustrating this idea for both regions.

Also, Fig. 1 shows the room temperature fit using Chow's model for asymmetric tunnel barrier, where the experimental curve can hardly be differentiated from the fitted one. This

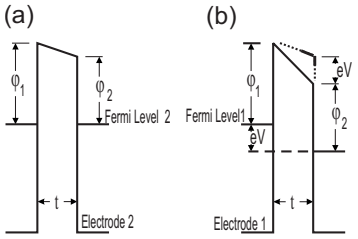

FIG. 2. (a) Schematic energy diagram for low voltage region $V \to 0$ and (b) for intermediate voltage region $0 \leqslant V \leqslant \varphi_2$. Electrode 2 is positively biased with respect to electrode 1.

I-V curve behavior can be reasonably well described also by Simmons' model, on account of the small potential asymmetry. The values obtained by the fitting procedures, for a group of samples, are shown in Table I. Several aspects of these parameters merit to be addressed.

First, under our experimental conditions, neither the barrier height nor its thickness is strongly affected by the oxidation time. We interpret this as a signature of the presence of hot spots. The *mean* oxide thickness, measured with low angle x-ray diffraction, increases almost linearly with oxidation time, but this will not be relevant for the tunneling when the current concentrates in small portions of the sample. As can be seen in Table I, the effective tunneling areas extracted from the fittings represent less than 1% of the junction's geometrical area, a percentage that is near those found by scanning tunneling microscopy. The extracted values for barrier thickness are around 10 Å, smaller than the values usually reported for similar junctions but close to those extracted by fitting of *I-V* curves measured using scanning tunneling microscopic tips.[27]

It should be mentioned here that considering the effective tunneling area in the fitting procedure limits the errors induced by interface roughness, as has been proved by modeling and simulations.[19] If the values obtained for all the samples are put together, they compose a consistent picture, showing the expected exponential growth of the normalized resistance (RA_{eff}) versus effective barrier thickness (t_{AlO_x}), as depicted in Fig. 3 for data taken from Table I corresponding

TABLE I. Barrier's intrinsic parameters extracted from fittings of *I-V* curves using Simmons' (Refs. 22–24) and Chow's models (Ref. 25). Barrier effective thickness (t_{AlO_x}), barrier potential height (φ), effective tunneling area (A_{eff}), and oxidation time (T_{ox}). *I-V* curves measured at 300 K and ferromagnetic electrodes in the antiparallel state of magnetization.

	Symmetric barrier				Asymmetric barrier	
	Simmons		Chow		Chow	
T_{ox} (s)	φ_0 (eV)	t_{AlO_x} (Å)	φ_0 (eV)	A_{eff} (cm^2)	φ_1 (eV)	φ_2 (eV)
30	0.726±0.014	8.98±0.08	0.778±0.017	$(2.9\pm0.4)\times10^{-9}$	1.221±0.018	0.985±0.014
30	0.743±0.004	9.39±0.08	0.827±0.006	$(1.9\pm0.3)\times10^{-9}$	1.239±0.015	1.032±0.019
30	0.807±0.023	9.96±0.18	0.914±0.035	$(1.2\pm0.4)\times10^{-8}$	1.231±0.025	0.990±0.011
45	0.819±0.021	10.14±0.20	0.926±0.032	$(2.1\pm0.3)\times10^{-8}$	1.236±0.024	1.002±0.023
45	0.793±0.006	10.53±0.07	0.945±0.013	$(1.1\pm0.1)\times10^{-8}$	1.251±0.013	1.018±0.022
60	0.836±0.024	10.98±0.11	0.990±0.017	$(3.9\pm0.4)\times10^{-8}$	1.269±0.011	1.034±0.017
60	0.845±0.0009	11.71±0.20	1.039±0.007	$(3.5\pm0.7)\times10^{-8}$	1.308±0.029	1.075±0.025

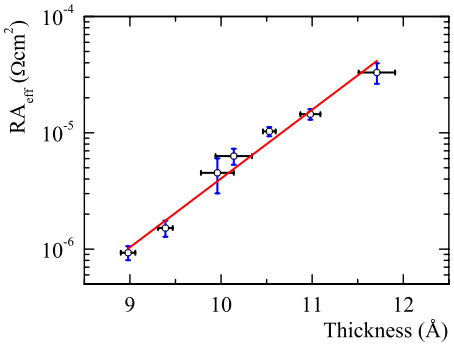

FIG. 3. (Color online) Room temperature effective area resistance product (RA_{eff}) as a function of the tunneling effective barrier thickness (t_{AlO_x}). Low voltage electrical resistance determined in the linear range of *I-V* curves between −40 and +40 mV. The continuous line has been calculated according to the expression $P\exp[(2t_{\text{AlO}_x}/\hbar)\sqrt{2m\varphi_0}]$, where $P=7.4\times10^{-12}\ \Omega\ \text{cm}^2$ and $\varphi_0=1.4$ eV. For this expression, the potential barrier height (φ_0) is an independent function of t_{AlO_x}, and the effective mass of the tunneling electron within the barrier is neglected.

to Chow's model for symmetric tunnel barrier.

The last two columns on the right hand side of Table I show the potential barrier heights φ_1 and φ_2 for asymmetric tunnel barrier, as shown in Fig. 2, where φ_1 and φ_2 are the potential barrier height at the first and second metal/insulator/metal interfaces, respectively. The asymmetry ($\Delta\varphi$) is roughly 0.2 eV, meaning that the MTJs have an almost rectangular potential barrier.

Figure 4 shows the derivative of a fitted *I-V* curve as a function of applied bias. This is a parabolic curve slightly shifted to negative values of bias with minimum conductance at $V_{min}=-11.87$ mV, as can be verified in the inset of Fig. 4 (see the arrow), where the second derivative is plotted around the position of the minimum. This slight shift is due

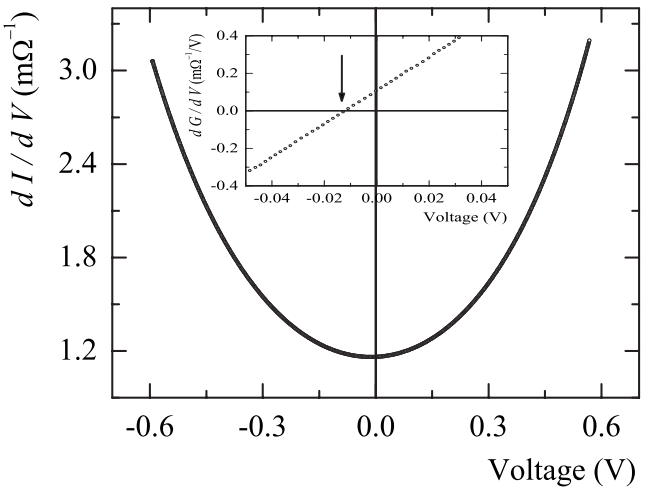

FIG. 4. Derivative of a fitted *I-V* curve as a function of the applied bias for a Py/Al(20 Å)O_x(30 s)/Co MTJ. Note that the curve is slightly shifted to the left as can be seen in the inset for the second derivative. No magnetic field was applied during the measurement at 300 K.

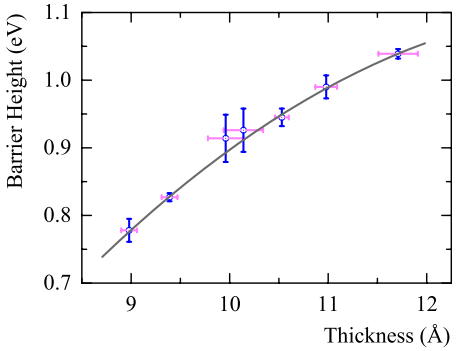

FIG. 5. (Color online) Room temperature potential barrier height as a function of the tunneling effective barrier thickness (t_{AlO_x}). The continuous line is only a guide to the eyes.

to a low asymmetry potential barrier, usually correlated to MTJs with properly oxidized tunnel barriers and an almost rectangular potential barrier height ($\varphi_1\approx\varphi_2$).[28] This also justifies why simulations for symmetric tunnel barrier show good agreement with experimental *I-V* curves for both models.

As can be seen on Table I, for Simmons' and Chow's model simulations, we have values of $\varphi\leqslant1.0$ eV, meaning that we have deposited samples with low potential barrier height values, if compared to values reported in the literature for the same system ($\varphi\geqslant1.9$ eV).[29,30] We can argue about the physical reasons for this low potential barrier. It could be due to deviation from Al_2O_3 stoichiometry in the regions relevant for the tunneling transport. Up to now, we do not have an experimental method to follow locally the composition of the oxide.

Another possibility is that a buildup process of the tunnel barrier is present. Figure 5 shows the potential barrier height as a function of thickness using the values from Table I corresponding to Chow's model for symmetric barrier. We can see an increase of the barrier height for increasing thickness. This trend could be an indication that for very thin oxide layers, the insulator gap has not yet been completely established. In junctions with Al electrodes[31] where the tunneling barrier was produced under the same experimental conditions as the MTJs, barrier height values increases toward saturation in a figure slightly smaller than the Al_2O_3 bulk reported values.

Figure 6 shows TMR-ac curves for different applied bias. As usual, TMR decreases with increasing bias, and it does much faster for ac (low frequencies) than dc measurement (not shown). Finally, TMR changes from positive to negative at a critical bias V_C that is almost independent from the polarity (nearly symmetrical curve), in contrast with what is observed in double insulating barrier or strongly asymmetric ones. This inversion of TMR is an uncommon behavior for this well-known positive system.

Some possibilities should be considered underlying the TMR inversion. From the DOS near the Fermi level point of view, no drastic change in the spin polarization has been predicted or measured for magnetic transition metals junctions when, by the applied bias, DOS above or under the original Fermi Level are probed by tunneling current.

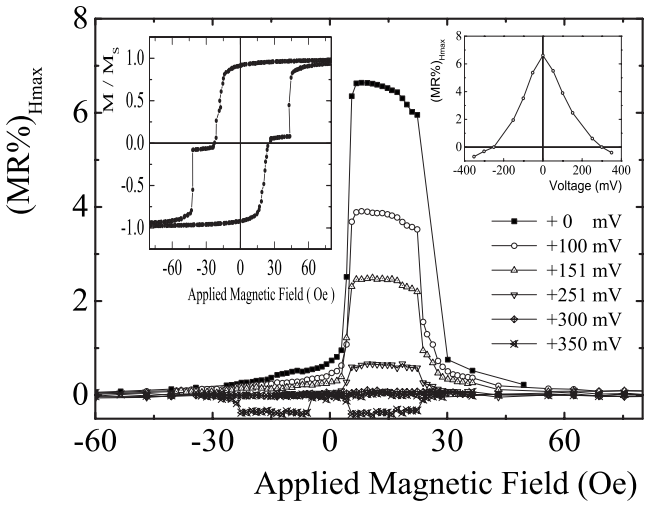

FIG. 6. TMR-ac curves for different applied biases for a Py/Al(20 Å)O_x(30 s)/Co MTJ at 77 K. Inset: magnetization as a function of the applied magnetic field showing a different coercive force for a Py/Al(20 Å)O_x(60 s)/Co MTJ. The figure also shows the magnetoresistance bias dependence for the Py/Al(20 Å)O_x(30 s)/Co MTJ.

As the tunnel current is concentrated in hot spots, current densities can reach relatively high values (5.6×10^5 A/cm^2). For very low potential barrier height such as MgO (0.34–0.50 eV), Beletskii *et al.*[12] have shown that current densities can be increased up to 10^6 A/cm^2 and thus switch the magnetization of the free ferromagnetic layer. However, a similar mechanism in the present case is very unrealistic. As the magnetic material above or under the hot spots regions is coupled by direct magnetic exchange with the rest of the electrode, any inversion would demand quite large current densities,[32] 2 orders of magnitude larger than those estimated here. Finally, this extrinsic effect must be dismissed because, even if it could induce some decreasing with bias voltage increasing, it could not generate any inversion in the TMR signal.

A simple Slonczewski type parabolic band model, valid for $V \rightarrow 0$, supports an effective negative spin polarization coefficient (P) value due to low potential barrier height effect, which would be a qualitative explanation for this behavior.[8] In the present case, the inversion of TMR as a function of the barrier potential height can be understood in the framework of the Li and co-workers[9–11] model for the intermediate voltage range (experimentally measurable). This treatment is an extension of Slonczewski's model for finite bias, where the barrier's potential height presents a strong bias dependence. As pointed out, TMR can be expressed [Eq. (14) in Ref. 11] as a function of the quantum coherence factor by

$$\mathrm{TMR} \propto \sum_{k_1} \int_{-\infty}^{+\infty} dE_x A(E_x,V) D(E_x,V) \exp[-2\eta(E_x,V)] \times [F(E) - F(E-eV)], \tag{7}$$

where the summation over k_1 stands for the contribution from the lateral (in plane) parts of the Hamiltonians, E for the total energy of the tunneling electrons, $f(E)$ for the Fermi distribution function, and $\exp[-2\eta(E_x,V)]$ for the exponential weighting factor in the WKB approximation.

The factor $A(E_x,V)$ is the DOS contribution from the ferromagnetic electrodes and is always positive, no matter the magnitude of the bias. Thus, it does not contribute to the TMR inversion as mentioned above.

The quantum coherence factor [Eq. (47) in Ref. 9] is given by

$$D(E_x,V) = \left(\frac{2m}{\hbar^2}\right)[(\varphi_2 - E_x - eV) - \sqrt{(E_x+eV)^2 - \Delta^2}], \tag{8}$$

where Δ stands for one-half of the exchange splitting between the two spin bands of the ferromagnetic electrodes, V for the applied bias, E_x for the longitudinal part of the electron energy, m for the electron mass, and φ_2 for the potential barrier height at the second barrier/electrode interface (see Fig. 2). The first term on the right hand side is the potential barrier height contribution and the second one is the transmission coefficient contribution. The former decreases with the increase of the bias and the latter increases with V, so the quantum coherence factor is a rapidly decreasing function of V. As the bias increases, this factor will drop to zero and then become negative beyond a critical voltage V_C.

This physical mechanism is responsible for the decrease and change of sign of the quantum coherence factor at the intermediate voltage range. The only factor in Eq. (7) capable of decreasing and inverting the TMR due to the applied bias is the quantum coherence. The effect originates from the low potential barrier height and the transmission coefficient rather than the DOS contribution. It means that the lower (higher) the potential barrier height, the smaller (larger) the TMR. Also, the larger the transmission coefficient, the lower the TMR. This could explain why a high potential barrier such as Al_2O_3 does not show TMR inversion (before dielectric breakdown is reached), while a low potential barrier such as Ta_2O_5 (φ=0.4 eV) does.[14]

To check if the quantum coherence is the dominant mechanism behind the inversion here observed, we could estimate the critical voltage beyond which TMR is negative. At zero temperature, with barrier height of ~1 eV, chemical potential defined as the energy level at the middle of the insulating barrier, and 1.4 eV for the splitting of Co spin up spin down bands, we find $V_C \approx 250$ mV, which is close to the measured values. However, it should be emphasized that this is a quite crude approximation as, besides the intrinsic limits of applicability of parabolic band type models to 3d metals, we are also neglecting effects of electron effective mass inside the barrier, magnon excitations, and other temperature effects.

The most robust results supporting the quantum coherence factor role in the TMR inversion are presented in Fig. 7, showing a slight increase of the measured critical voltage with the barrier height, in accordance with the linear prediction.[33] Also, the small asymmetry observed in the

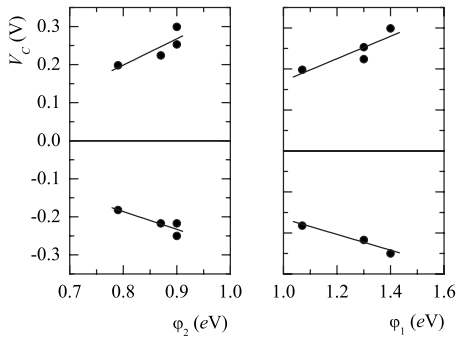

FIG. 7. Critical voltage as a function of the potential barrier height showing a linear behavior and supporting the quantum coherence factor role in the TMR inversion as predicted in the model of Fei-Fei *et al.* (Ref. 33). Measurement made at 77 K.

TMR-ac curves for different applied bias follows the slight difference between the potential heights at both sides of the barrier.

Usually, for Al_2O_3 tunnel barrier, the potential height is high and its critical voltage V_C is so large that the junction will break down before inversion of the TMR is observed. The Fermi level is too far below the effective barrier height and the rate of tunneling electrons as well as the transmission coefficient are lower when compared to a low potential barrier height at the same applied bias. In the present case, with low potential barriers for the same insulating material, the critical voltage V_C is small enough to observe inversion of the TMR before the breakdown voltage. Finally, as the TMR depends on potential barrier height, this could explain why our MTJs show lower TMR values (up to 8% at 77 K) than those reported by other authors.[29]

IV. CONCLUSIONS

The good agreement for the fitting of *I-V* curves suggest that although Simmons' and Chow's models are based on free electron approximation, both can capture the main aspects of the physics involved in tunnel junctions with ferromagnetic electrodes. We can therefore conclude that assumptions made in both models still lead to coherent results in the MTJs deposited under our specific experimental conditions. A_{eff} values indicate the presence of a nonuniform current distribution.

We have found TMR inversion for a widely known positive system such as $Py/AlO_x/Co$, where no inversion would be expected arising from the DOS for both electrodes. As our specific experimental conditions result in insulating barrier with low height and low asymmetry, we conclude that the almost symmetrical TMR versus voltage bias curves and the TMR inversion in this system is in agreement with the model of Li and co-workers,[9–11] which predicts inversion of TMR due to low potential barrier height effects.

ACKNOWLEDGMENTS

This work has been partially supported by Conselho Nacional de Desenvolvimento Científico e Tecnológico (CNPq) and Centro Latinoamericano de Física (CLAF).

*Author to whom correspondence should be addressed. mbaibich @if.ufrgs.br

[1] W. Wulfhekel, H. F. Ding, and J. Kirschner, J. Magn. Magn. Mater. **242-245**, 47 (2002).
[2] P. LeClair, J. T. Kohlhepp, C. H. van de Vin, H. Wieldraaijer, H. J. M. Swagten, W. J. M. de Jonge, A. H. Davis, J. M. MacLaren, J. S. Moodera, and R. Jansen, Phys. Rev. Lett. **88**, 107201 (2002).
[3] I. I. Mazin, Phys. Rev. Lett. **83**, 1427 (1999).
[4] X. H. Xiang, T. Zhu, J. Du, G. Landry, and J. Q. Xiao, Phys. Rev. B **66**, 174407 (2002).
[5] J. Zhang and R. M. White, J. Appl. Phys. **83**, 6512 (1998).
[6] S. Zhang, P. M. Levy, A. C. Marley, and S. S. P. Parkin, Phys. Rev. Lett. **79**, 3744 (1997).
[7] G. G. Cabrera and N. García, Appl. Phys. Lett. **80**, 1782 (2002).
[8] J. C. Slonczewski, Phys. Rev. B **39**, 6995 (1989).
[9] F. F. Li, Z. Z. Li, M. W. Xiao, J. Du, W. Xu, and A. Hu, Phys. Rev. B **69**, 054410 (2004).
[10] R. Yuan, Z. Z. Li, M. W. Xiao, and A. Hu, J. Phys.: Condens. Matter **17**, 4121 (2005).
[11] F. F. Li, Z. Z. Li, M. W. Xiao, D. Jun, X. Wang, and A. Hu, J. Appl. Phys. **95**, 7243 (2004).
[12] N. N. Beletskii, G. P. Berman, S. A. Borysenko, S. A. Wolf, and V. M. Yakovento, J. Appl. Phys. **101**, 074305 (2007).
[13] N. N. Beletskii, G. P. Berman, A. R. Bishop, S. A. Borysenko, and V. M. Yakovento, Phys. Rev. B **75**, 174418 (2007).
[14] M. Sharma, S. X. Wang, and J. H. Nickel, Phys. Rev. Lett. **82**, 616 (1999).
[15] S. Yuasa, T. Nagahama, and Y. Suzuki, Science **297**, 234 (2002).
[16] S. Yuasa, T. Sato, E. Tamura, Y. Suzuki, H. Yamamori, K. Ando, and T. Katayama, Europhys. Lett. **52**, 344 (2000).
[17] L. S. Dorneles, D. M. Schaefer, M. Carara, and L. F. Schelp, Appl. Phys. Lett. **82**, 2832 (2003).
[18] Philip C. D. Hobbs, Robert B. Laibowitz, and Frank R. Libsch, Appl. Opt. **44**, 32 (2005); **44**, 6813 (2005).
[19] Casey W. Miller, Zhi-Pan Li, Joham Akerman, and Ivan K. Schuller, Appl. Phys. Lett. **90**, 043513 (2007).
[20] V. Da Costa, C. Tiusan, T. Dimopoulos, and K. Ounadjela, Phys. Rev. Lett. **85**, 876 (2000).
[21] J. D. R. Buchanan, T. P. A. Hase, B. K. Tanner, N. D. Hughes, and R. J. Hicken, Appl. Phys. Lett. **81**, 751 (2002).
[22] J. G. Simmons, J. Appl. Phys. **34**, 1793 (1963).
[23] J. G. Simmons, J. Appl. Phys. **35**, 2655 (1964).
[24] J. G. Simmons, J. Appl. Phys. **34**, 2581 (1963).
[25] C. K. Chow, J. Appl. Phys. **36**, 559 (1965).
[26] T. Miyazaki and N. Tezuka, J. Magn. Magn. Mater. **151**, 403 (1995).
[27] V. Da Costa, Y. Henry, F. Bardou, M. Romeo, and K. Ounadjela, Eur. Phys. J. B **13**, 297 (2000).
[28] J. Nowak, J. Appl. Phys. **87**, 5203 (2000).

[29] J. S. Moodera, L. R. Kinder, T. M. Wong, and R. Meservey, Phys. Rev. Lett. **74**, 3273 (1995).
[30] H. Boeve, E. Girgis, J. Schelten, J. De Boeck, and G. Borghs, Appl. Phys. Lett. **76**, 1048 (2000).
[31] L. S. Dorneles, Ph.D. thesis, Universidade Federal de Santa Maria, 2003, http://planeta.terra.com.br/educacao/lsdorneles/tese/.
[32] Yisong Zhang, Zhongzhi Zhang, Yaowen Liu, Zhixiong Kang, B. Ma, and Q. Y. Jin, J. Appl. Phys. **101**, 103905 (2007).
[33] F. F. Li, Z. Z. Li, and M. W. Xiao, Chin. Phys. **14**, 1025 (2005).